Tuning electrical properties in Ga_2O_3 polymorphs induced with ion beams

A.Y. Polyakov[1], A. I. Kochkova[1], A. Azarov[2], V. Venkatachalapathy[2], A.V. Miakonkikh [3], A.A. Vasilev[1], A.V. Chernykh[1], I.V. Shchemerov[1], A.A. Romanov[1], A. Kuznetsov[1**] and S.J. Pearton[4*]

[1.] National University of Science and Technology MISiS, 4 Leninsky Avenue, Moscow 119049,

[2]Department of Physics/ Centre for Materials Science and Nanotechnology, University of Oslo, Problemveien 7, 0315 Oslo, Norway

[3]Valiev Institute of Physics and Technology, Russian Academy of Sciences (Valiev IPT RAS), Moscow, 117218, Nahimovsky Ave, 36(1), Russia

[4.] Department of Materials Science and Engineering, University of Florida, Gainesville, FL 32611, USA

*Corresponding author: E-mail:spear@ mse.ufl.edu

**Corresponding author:andrej.kuznetsov@fyz.uio.no

ABSTRACT

Ion beam fabrication of metastable polymorphs of Ga_2O_3, assisted by controllable accumulation of the disorder in the lattice, is an interesting alternative to conventional deposition techniques. However, the adjustability of the electrical properties in such films is unexplored. In this work we investigated two strategies for tuning the electron concentration in the ion beam created metastable κ-polymorph: adding silicon donors by ion implantation and adding hydrogen via plasma treatments. Importantly, all heat treatments were limited to ≤ 600^{o}C, set by the thermal stability of the ion beam fabricated polymorph. Under these conditions, silicon doping did not change the high resistive state caused by the iron acceptors in the initial wafer and residual defects accumulated upon the implants. Conversely, treating samples in a hydrogen plasma converted the ion beam fabricated κ-polymorph to n-type, with

a net donor density in the low 10^{12} cm^{-3} range and dominating deep traps near 0.6 eV below the conduction band. The mechanism explaining this n-type conductivity change may be due to hydrogen forming shallow donor complexes with gallium vacancies and/or possibly passivating a fraction of the iron acceptors responsible for the high resistivity in the initial wafers.

I.INTRODUCTION

Ga_2O_3 is a wide-bandgap semiconductor under intense study for applications in new generation of devices for power electronics and far-UV photodetectors [1-3]. Until recently, most attention has focused on the thermodynamically stable monoclinic β-Ga_2O_3 polymorph with bandgap of 4.8 eV for which very promising device performance has been demonstrated [1-3]. However, as for many wide-bandgap semiconductors, Ga_2O_3 is characterized by the existence of several metastable polymorphs among which the corundum structure α-Ga_2O_3 and orthorhombic κ-Ga_2O_3 [1] also attract recent attention. One more polymorph of practical importance is called γ-Ga_2O_3 [1]. This is a defective spinel cubic phase in which the Ga sites are only partially occupied, with varying ratio of octahedra and tetrahedra sites [4]. The state of advancement of these polymorphs is at present very different. While for α-Ga_2O_3 with the bandgap of 5.2 eV, reasonably high quality films can be prepared on sapphire by various epitaxial approaches [1, 5-8] and viable power rectifiers with Schottky barrier gates, alongside with useful p-n heterojunctions have been demonstrated [5-8], the situation with high crystalline quality growth and electrical properties characterization for κ-Ga_2O_3 has not been so advanced.

κ-Ga_2O_3 has a bandgap only slightly lower than β-Ga_2O_3 (4.6 eV versus 4.8 eV), but has an important advantage over the latter in that it has a strong spontananeous electrical polarization, much exceeding that of the III-Nitride compounds. This has promise for attaining very high two-dimensional electron gas (2DEG) or hole gas (2DHG) density in κ-Ga_2O_3 heterojunctions via ”polarization doping” . This in turn could lead to heterojunction field effect transistors with current handling capability exceeding that of III-N devices at higher break-down voltages if the high crystalline quality of the material is realized [1,2, 9,10].

The interest in the γ-Ga_2O_3 polymorph stems from recent observations that point to the γ-polymorph forming as a transitory phase when α-Ga_2O_3 and κ-Ga_2O_3 are transformed into the stable β-Ga_2O_3 upon high temperature annealing at temperatures > 700-800ºC [4]. An interesting feature of β-Ga_2O_3 is that, when implanted with high doses of ions, the material in the implanted region does not undergo amorphization as in many other semiconductor materials, but rather changes to metastable polymorphs, the nature of which is currently under some debate. It has been reported that Si implantation with high doses converts β-Ga_2O_3 to κ-Ga_2O_3 [11,12] that then is transformed into β-Ga_2O_3 at >700-800ºC. However, it has also been suggested that implantation with high Si doses results in the formation of the mixture of κ-Ga_2O_3 and γ-Ga_2O_3 polymorphs that turns into γ-Ga_2O_3 and then β-Ga_2O_3 under increasingly higher temperature anneals [13], although contray reports exist[14].

The problem with capitalizing on the promising properties of κ-Ga_2O_3 for achieving polarization doping in transistors is that, when epitaxially grown, it tends to form microdomains rotated by 120º thus resulting in a high grain boundary defect density and poor in-plane electrical conductivity [4, 10]. Recently, advances in crystalline quality of κ–Ga_2O_3 films have been achieved via using epitaxial lateral overgrowth [15], growth of very thick κ-Ga_2O_3 layers by Halide Vapor Phase Epitaxy (HVPE) [16] or using growth on high-crystalline quality isomorphouse $GaFeO_3$ substrates [17].

Yet another possibility is where the formation of a new phase provisionally identified as κ-Ga_2O_3 has been reported to be the result of ion implantation of Ni, Ga, or Au with high doses [18]. The observed phenomenon was attributed to the fact that the formation of κ-Ga_2O_3 is strongly favored by high strain in the material, as evidenced by studies of films grown on heavily lattice mismatched substrates such as diamond, SiC, AlN, GaN [19, 20]. If the assignment proposed in Ref. [1] is correct, this could offer in principle a new way of

fabricating κ-Ga_2O_3/β-Ga_2O_3 heterojunctions with a possible advantage that this could be done in the very high crystalline quality β-Ga_2O_3 material.

However, in order for that approach to be of practical interest one needs a) to assess the effect of radiation damage caused by ion implantation on the electrical properties of the newly formed polymorph; b) to find a way to control the electrical properties of the layer in order to be able to practically use the effect. These tasks were addressed by studying the electrical properties of semi-insulating β-Ga_2O_3 crystals compensated with Fe and implanted with Ga ions. The strategy of getting the implanted material conducting was two-pronged. One direction investigated was to implant the Ga-implantation modified material with high doses of Si and try to activate Si donors by anneals at temperatures not exceeding those that convert the κ-Ga_2O_3 polymorph into γ-Ga_2O_3 or β-Ga_2O_3. The other approach was to subject the implanted material to treatment in hydrogen plasmas, shown to promote hydrogen complex formation with Ga vacancies and partial passivation of compensating Fe acceptors. These processes are expected to result in the formation of n-type conductivity [21].

In this paper, we demonstrate that the latter approach, treatment of implanted β-Ga_2O_3 in H plasmas, leads to a partial success in that n-type conductivity can be achieved while annealing of Ga and Si implanted samples at temperatures up to 600^{o}C does not give rise to measurable n-type doping. We briefly discuss possible limitations and ways to increase the donor density achieved.

II.EXPERIMENTAL

We used semi-insulating Fe-doped (010) β-Ga_2O_3 single crystals from Tamura Corp. [22]. To form a phase-modified surface layer, the initial implantation was performed at room temperature (RT) with 1.7 MeV Ga ions to a fluence of 6×10^{15} cm^{-2}. After that, additional implants with Si ions were performed at RT, 200 °C and 400 °C to fabricate the near- surface doped layer. The energies and doses of Si ions were chosen to get a box-like profile. The

implant parameters including ion type, energy, dose and implantation temperature (T_i) are summarized in Table 1.

The structural quality of the implanted samples was characterized by a combination of Rutherford backscattering spectrometry in channeling mode (RBS/C) [18] and x-ray diffraction (XRD) measurements. RBS/C measurements were performed using 2.5 MeV He^{2+} ions incident along the [010] direction and backscattered into a detector placed at 165° relative to the incident beam direction. XRD Θ-2Θ measurements were performed using the Bruker AXS D8 Discover diffractometer with high-resolution Cu $K_{\alpha 1}$ radiation.

For electrical characterization, four Ohmic contacts were prepared by deposition of Ti/Al and Schottky diodes made by deposition of Ni. The samples were then characterized by van der Pauw conductivity measurements, current-voltage (I-V) measurements between the Ohmic contacts and between the Schottky and Ohmic contacts, current versus temperature measurements, capacitance versus frequency (C-f) measurements, capacitance versus voltage (C-V) profiling, admittance spectra measurements (AS) [23], Photoinduced Current Transient Spectroscopy (PICTS) [24], Current Deep Level Transient Spectroscopy (CDLTS) [25], and by capacitance Deep Level Transient Spectroscopy (DLTS) [23].

Ohmic contacts and Schottky contacts were fabricated by e-beam evaporation, the thickness of the Ti/Al bi-layer was 20 nm/80 nm, the thickness of the Ni layer was 20 nm. The Ohmic contacts were deposited at the four angles of the square 5mm× 5mm samples, the circular Schottky diodes of 1 mm in diameter were deposited in the center of the samples in between the Ohmic contacts. I-V, C-f, C-V, DLTS measurements were performed in the dark or with monochromatic illumination using a set of light emitting diodes (LEDs) with wavelength ranging from 259 to 940 nm in the temperature range 77-500K. Capacitances were measured at frequencies from 20Hz to 20 MHz and DLTS spectra were monitored using the probing frequency corresponding to the plateau of the C-f dependence. The probing

frequency could be set between 1 kHz and 1 MHz, the measured capacitance relaxation curves were corrected by changes of the capacitance values during capacitance transients. The setups of such DLTS or Optical DLTS measurements are described elsewhere [21, 26-29]. The samples were measured immediately after implantation of Ga or Ga+Si and after annealing between 200º-600ºC.

Since these heat treatments were not sufficient to activate the electrical conductivity of the samples, we also tried a treatment in dense hydrogen plasma in the hope that hydrogen complexes with radiation defects, in particular, Ga vacancies [21], could introduce shallow donor centers without destroying the κ-Ga_2O_3 layer induced by Ga implantation.

This hydrogen plasma treatment was performed in an Inductively Coupled Plasma (ICP) reactor (Plasma Lab 100 dual, Oxford Instruments Technology, UK) at 330ºC for 30 min., at a pressure of 36 mTorr. The ICP RF power was 1500W, the RF power applied to the chuck was 75 W and the bias on the chuck was 298 V [21].

III.RESULTS AND DISCUSSION

The structural changes occurring in the Ga_2O_3 samples due to implantation are illustrated by Fig. 1 showing the (a) RBS/C spectra and (b) corresponding XRD Θ-2Θ scans of the samples before and after implantation. From Fig. 1(a), Ga implantation produced a surface modified layer with thickness ~1 μm. The channeling yield in this layer corresponds to ~90% of the random level and, according to the previous results [18], this layer corresponds to the new phase of Ga_2O_3. The phase transformation is also supported by XRD results (Fig. 1(b)) showing the new diffraction peak located at 63.7 degrees which appears after implantation. Implantation also leads to the prominent broadening of the (020) β-Ga_2O_3 diffraction peak, indicating formation of some strain and defects in the interface region. Based on combined RBS/C, XRD, and Transmission Electron Microscopy results, this phase has been identified as κ-Ga_2O_3 [18].

Additional Si implants were performed to make a box-like Si profile in the phase-modified layer and the Si concentration versus depth profile was formed within the new phase, extending to the 400 nm from the surface with peak concentration of about 5×10^{19} cm^{-3}, according to the SRIM code [30] simulations (see Fig. 1(a)). These Si implants led to a decrease of the channeling yield in the near surface region, indicating some improvement of the crystalline quality in the implanted region. Furthermore, the thickness of the phase-modified layer decreased with increasing implantation temperature and its thickness became ~940 nm after Si implantation at 400 °C (see Fig. 1(a)). Moreover, the RBS/C data indicate that the sharpness of the inner interface between the new and β-phases improves. According to the XRD data, the new phase still persists even after 400 °C (Fig. 1(b)) and high temperature Si implantation leads to the increase of the sharpness of the (020) β-Ga_2O_3, corroborating the RBS/C results.

The thermal evolution of the phase modified layer in the Ga+Si (200 °C) co-implanted samples is illustrated by Fig. 2, showing the RBS/C spectra of the sample before and after annealing. Annealing led to the shrinkage of the layer and its thickness was 890 nm after 500 °C anneal. Electrical measurements for the as-implanted with Ga samples were not feasible: the current was extremely low and the capacitance of the Schottky diodes was not measurable. The sample additionally implanted with Si at room temperature was also not informative. For the samples implanted with Si at 400°C the dark current was still very low, but it increased at higher measurement temperature. The sample also showed a measurable photocurrent. Fig. 3(a) shows the room temperature and 400K I-V characteristics of the sample measured between the Ohmic contacts in the dark and the I-V characteristic measured at room temperature with 277 nm wavelength (4.5 eV photon energy) UV LED excitation. The spectral dependence of the photocurrent under the excitation with LEDs with different photon energies is shown in Fig. 3(b) (the optical power density for the LEDs with photon

energies up to 3.4 eV was 250 mW/cm^2, the power output density for the 4.5 eV LED was 25 mW/cm^2).

The measurable photocurrent appeared for photons with energy 1.5 eV and strongly increases for photons with energy 2.3 eV. The photocurrent for photon energies of 2.3 eV was persistent, while for photon energies above 2.8 eV, the photocurrent rapidly returned to the starting value corresponding to the 2.3 eV excitation once the LED was switched off (open squares in Fig. 3(b) show the photocurrent with the LED turned on, solid squares display the photocurrent measured after 10 minutes after the switching off of the excitation light). Fig. 3(c) displays the current at 50V temperature dependence measured upon heating up after illumination at room temperature with 4.5 eV LED for 10 minutes (red line) and the temperature dependence measured from high temperature of 420K while cooling down. The heating up curve shows a slight growth of current with activation energy of 0.4 eV, then a decrease of current and a new exponential increase with activation energy 0.5 eV. When cooling down from high temperature, the current exponentially decreased with temperature with activation energy of 0.8 eV. These are rather characteristic features of the Thermally Stimulated Conductivity (TSC) spectra [25] in which the conductivity after illumination increases as the states filled by light release the captured charge carriers and the activation energy at the rising current temperature dependence slope correspond approximately to the depth of the states capturing charge carriers (0.4 eV and 0.5 eV, most likely in relation to the conduction band edge). The activation energy measured upon cooling down after the heating up to high temperature corresponds to the position at which the Fermi level is pinned in the dark (near E_c-0.8 eV).

For the sample implanted with Si at 200^{o}C and annealed up to 600^{o}C, the characteristics were similar to the unannealed sample in terms of dark current, photocurrent values and photocurrent spectra and in terms of the current temperature dependences upon heating from

room temperature after illumination and subsequent cooling down from high temperature, with the slight difference in optical thresholds for photocurrent (2 eV and 2.8 eV) and in the energy of the states revealed in TSC spectra (trapping states near 0.4 eV and 0.7 eV and the Fermi level pinning position near E_c-0.9 eV (see Supplementary Material, Fig. S1(a, b, c)).

Some additional information could be gleaned from PICTS spectra measured with 4.5 eV LED excitation with different lengths of the probed relaxation times and temperatures. Fig. 4 (a) shows such spectra for the sample implanted with Ga and implanted with Si at 400^{o}C for short probed relaxation times up to 17 s. Unexpectedly, the peaks in PICTS spectra shift to higher temperatures as the time window in PICTS becomes longer. In simple PICTS theory, the position of the peak in the PICTS signal $\Delta I(PICTS)/I_{ph}= (I(t1)-I(t2))/I_{ph}$ corresponds to the condition $1/t1=e_n(T_M)$, where t1and t2 are time windows (t2>>t1), T_M is the peak maximum, I_{ph} is the steady-state photocurrent, and e_n is the trap emission rate [24]). Thus, under normal circumstances the peak position in PICTS shifts to lower temperatures as the t1 value becomes longer. This is obviously not the case for the samples in which the peak shifts to higher temperatures for increasing t1. The activation energy calculated from the equation above is negative and ~ 0.4 eV. Moreover, the analysis of the relaxation curves in PICTS shows that they are stretched exponents of the kind $I=I_o\exp[(-t/\tau)^{\beta})]$ rather than simple exponents often observed in PICTS [24]. Fig. S2(a) in the Supplementary Material shows several relaxation curves measured in PICTS spectra at different temperatures that have been fitted by the stretched exponents whose characteristic lifetimes change with temperature as shown in Fig. S2(b) and the broadening parameter changes as displayed by Fig. S2(c) of the Supplementary Material. The characteristic lifetime still unusually becomes longer with increasing temperature and shows a negative activation energy of -0.2 eV.

The relaxation of photocurrent in the form of extended exponents is a hallmark of processes involving prominent potential fluctuations or recombination in the presence of

potential barriers for capture of charge carriers [31]. The nature of these processes is not clear at the moment, but it is interesting the relaxation times t change with temperature with activation energy similar to the difference in the bandgap energies of the β-Ga_2O_3 and κ-Ga_2O_3 polymorphs. However, if one analyzes the spectra measured with very long relaxation tmes at higher temperatures, the sign of the PICTS peak becomes negative, the position of the peak shifts in the right direction with increasing the time window, and the activation energy becomes high, 1.4 eV (Fig. 4(b)). The nature of underlying processes needs further study, but the latter energy is close to the one often observed for major hole traps in PICTS and ODLTS in β-Ga_2O_3 [27] and attributed to some form of Ga vacancies [27].

The samples implanted with Ga and Si and annealed up to 600^{o}C show the formation of the κ-Ga_2O_3 phase, a high density of deep compensating traps presumably related to Fe acceptors [26] and Ga vacancies, prominent potential fluctuations, but no donor activation. Since annealing at higher temperatures was expected to destroy the κ-Ga_2O_3 film produced by Ga implantation, we have tried to improve the situation with n-type doping by exposing the two samples, one subjected to Ga implantation, Si implantation at 400^{o}C (called henceforth Ga-Si-400C), the other implanted with Ga, implanted with Si at 200^{o}C and annealed to 600^{o}C (sample Ga-Si-200°C-600°C ann) to hydrogen plasmas at 330^{o}C for 30 minutes. The hope was that the formation of hydrogen complexes with Ga vacancies would contribute to the increase of shallow donor centers [21], with simultaneous decreasing the number of compensating acceptors due to Ga vacancies produced by irradiation and due to Fe acceptors that have been shown to be passivated by hydrogen in our earlier experiments with H plasma treatments of β-Ga_2O_3 [21].

The results of optical and electrical characterization for both samples after such H plasma treatment unambiguously testify to the formation of the surface n-type layer. Fig. 5 shows I-V characteristics of the sample Ga-Si-400C (implanted with Ga at room temperature

and with Si at 400°C, unannealed) at three temperatures. The data clearly indicate n-type conductivity with high series resistance (8×10^5 Ω at room temperature) (see Fig. 5(a)) increasing for lower temperature and decreasing for high temperature, measurable capacitance at room temperature that increases under illumination (Fig. 5(b)), and effective net donor density near the surface ~2×10^{12} cm^{-3}, as follows from the capacitance versus voltage $C^{-2}(V)$ plot (Fig. 5(c)). The temperature dependence of the forward current measured upon cooling in the dark from high temperature is 0.12 eV, which indicates the Fermi level pinning position in this n-type layer (Fig. 6). The sample shows prominent TSC after illumination at 300K with 4.5 eV photons, similar to that observed in the Ga and Si implanted sample (compare Fig.6 and Fig. 3(c)).

The spectral dependences of current (Fig. S3(a)) and capacitance (Fig. S3(b)) show the photosensitivity that is manifest in both reverse current and forward current and in photocapacitance on the C-f plateau. Respective spectral dependences of reverse current and capacitance on the frequency plateau are shown in Fig. 6. The former shows distinct optical thresholds near 2 eV and 2.8 eV and prominent persistent current . The optical thresholds in capacitance are shifted and capacitance also shows prominent persistent photocapacitance. One also observes systematic increase of the roll-off frequency in C-f characteristics due to the series resistance [23], which correlates with the decrease under illumination of the series resitance observed in forward I-V characteristics under illumination (see Fig. S4(a, b) in the Supplementary Material). The photocurrent spectra are similar to those in the Ga and Si implanted sample, with similar optical thresholds and similar persistent photocurrent behavior indicating the centers responsible are of the same nature.

We also performed admittance spectra measurements (i.e. the temperature dependences of capacitance, capacitance derivative on temperature dC/dT, AC conductance at different frequencies), CDLTS measurements and DLTS measurements for the H plasma

treated samples. Fig. 8(a) shows the temperature dependence of dC/dT for several frequencies, Fig. 8(b) displays the CDLTS spectra, Fig. 8(c) presents the DLTS spectra. The data for all three measurements point to the presence of deep traps with activation energy close to 0.6 eV. We have additionally tried ODLTS spectra measurements with 4.5 eV photon excitation, but these were still mostly determined by the presence of the 0.6 ev electron traps.

The results for the sample implanted with Si at 200ºC and annealed up to 600ºC were similar. The difference lies with a higher series resistance in forward direction ($3\times10^6\,\Omega$ versus $8.5\times10^5\,\Omega$ in the Ga-Si-400C), lower reverse current (Fig S5 of the Supplementary Material), lower roll-off capacitance frequency (Fig. S6 of the Supplementary Material), and lower photosensitivity in C-f and I-V (Fig. S7 of the Supplementary Material).

It is clear that the observed n-type conductivity has nothing to do with implanted Si donors because the concentrations are much lower than expected for the number of Si donors implanted and because they occur even without annealing that could facilitate activation of Si donors. Rather, the effect is due to the formation of complexes of hydrogen donors with structural defects formed by Ga and Si implantation, most likely complexes of hydrogen with Ga vacancies [32]. We have also reported that, under these H plasma treatment conditions, partial passivation of Fe acceptors occurs. The low net density of donors induced by H plasma treatment in our samples implies that the number uncompensated V_{Ga}-H complexes is low, which is the consequence of the presence of high density of Fe acceptors rendering the starting material semi-insulating (usually Fe concentrations around 10^{18} cm^{-3} are used [22]) and also the limited number of hydrogens incorporated during the plasma treatment and capable to form donor complexes with implantation defects. Partial annealing of such defects in the sample that underwent annealing up to 600ºC could explain the higher series resistance of this sample compared to the sample that was not annealed. This mechanism could be made

much more effective if the Fe acceptors concentration were greatly reduced and instead of trying to get n-type conductivity by ion implantation, one were to use Si doping during growth as in standard HVPE films. We have also reported that the amount of hydrogen and of hydrogen-related shallow donors can be strongly enhanced under our H plasma treatment conditions if the film or crystal orientation is (-201) instead of (010) were used [20], the reason being due to the existence of low-atomic density channels going inside the sample for the (010) orientation [21, 33].

SUMMARY AND CONCLUSIONS

We have shown that Ga implantation of (010) with a high dose of Ga or Ga and Si ions leads to the phase transformation of the top ~1 μm of the samples into a new phase, most likely κ-Ga_2O_3 polymorph. Si ion doping with subsequent annealing up to 600^{o}C allowing preservation of the κ-polymorph does not lead to measurable n-type conductivity. Instead, the material is highly resistive, with the Fermi level pinned near E_c-0.8 eV and with the presence of additional states with optical ionization thresholds near 1.5-2 eV and 2.8 eV and centers visible in TSC spectra with energies close to 0.4 eV and 0.5-0.7 eV. The photocurrent relaxation curves are stretched rather than simple exponents, which indicates either the presence of strong potential fluctuations, the existence of charge separation by a heterojunction (possibly the κ-Ga_2O_3/β-Ga_2O_3 heterojunction with bandgap difference ~0.2 eV) or the impact of centers with a measurable barrier for capture of charge carriers. The structures demonstrate pronounced persistent photoconductivity that survives above room temperature. The Si implantation and annealing does not seem to be a feasible way to fabricate operable κ-Ga_2O_3/β-Ga_2O_3 device structures unless a way can be found to preserve the κ-polytype for annealing temperatures ~1000^{o}C required for efficient activation of Si donors in Ga_2O_3 [34].

However, treating the implanted structures in a hydrogen plasma allowed achievement of n-type films, due most likely to formation of hydrogen complexes with radiation defects. The net donor concentrations were on the order of 10^{12} cm^{-3}, with a dominance of deep electron traps with levels at E_c-0.6 eV. Spectral dependences of photocapacitance and photocurrent point to the presence of deep compensating acceptors with optical thresholds similar to those observed in high-resistivity implanted films (centers with optical thresholds 2 and 2.8 eV and with prominent persistent photocapacitance and photocurrent). The factors limiting the net donor concentration achievable are the density of Fe acceptors that capture hydrogen, the density of hydrogen supplied from plasma, and the concentration of Ga vacancies available for the donor complexes formation with hydrogen. Optimization of the balance of these factors can substantially increase the net donor density that can be attained.

Supplementay Material

The material in the supplemental file shows additional electrical characterization of the κ-polymorph region after implantation or plasma treammnent to change the conductivity.

ACKNOWLEDGMENTS

The work at NUST MISiS was supported in part by a grant from the Ministry of Science and Higher Education of Russian Federation (Agreement # 075-15-2022-1113). The international collaboration was enabled by the INTPART program at the Research Council of Norway via project No. 322382. The work at UF was performed under the Interaction of Ionizing Radiation with Matter University Research Alliance (IIRM-URA), sponsored by Department of Defense, Defense Threat Reduction Agency under award HDTRA1-20-2-0002. The work at UF was also supported by NSF DMR 1856662 (James Edgar).

Data Availability

The data that supports the findings of this study are available within the article and its supplementary material.

Declarations

The authors have no conflicts to disclose.

REFERENCES

[1] Gallium Oxide: Materials Properties, Crystal Growth, and Devices, ed. Masataka Higashiwaki and Shizuo Fujita (Springer Series in Materials Science ISBN 978-3-030-37152-4, 2020).

[2] S. J. Pearton, Fan Ren, Marko Tadjer and Jihyun Kim, J. Appl. Phys. 124, 220901 (2018).

[3] J. Xu, W. Zheng and F. Huang. J. Mater. Chem. C, 7, 8753 (2019).

[4] I. Cora, Zs. Fogarassy, R. Fornari, M. Bosi, A. Recnik, B. Pécz, Acta Materialia 183 (2020) 216 (2020).

[5] Kentaro Kaneko, Shizuo Fujita, and T. Hitora, Japan J. Appl. Phys. 57, 02CB18 (2018).

[6] Elaheh Ahmadi, and Yuichi Oshima, J. Appl. Phys. 126, 160901 (2019).

[7] Alexander Y. Polyakov, Vladimir I. Nikolaev, Eugene B. Yakimov, Fan Ren, Stephen J. Pearton and Jihyun Kim, J. Vac. Sci. Technol. A 40, 020804 (2022).

[8] Kentaro Kaneko, Yasuhisa Masuda, Shin-ichi Kan, Isao Takahashi, Yuji Kato, Takashi Shinohe, and Shizuo Fujita, Appl. Phys. Lett. 118, 102104 (2021).

[9] A. Parisini, A. Bosio, V. Montedoro, A. Gorreri, A. Lamperti, M. Bosi,G. Garulli, S. Vantaggio, and R. Fornari, APL Mater. 7, 031114 (2019).

[10] H. von Wenckstern, Adv. Electron. Mater. 3, 1600350 (2017).

[11] T. Yoo, X. Xia, F. Ren, A. Jacobs, M. J. Tadjer, S. Pearton, and H. Kim, Appl. Phys. Lett. 121, 072111 (2022).

[12] Elaf A. Anber, Daniel Foley, A. C. Lang, J. Nathaniel, J. L. Hart, M. J. Tadjer, K. D. Hobart, S.J. Pearton and Mitra L. Taheri, Appl. Phys. Lett. 117, 152101 (2020).

[13] Hsien-Lien Huang, Christopher Chae, and Jinwoo Hwang, J. Appl. Phys. 131, 190901 (2022).

[14] Alexander Petkov, David Cherns, Wei-Ying Chen, Junliang Liu, John Blevins, Vincent Gambin, Meimei Li, Dong Liu, and Martin Kuball, Appl. Phys. Lett. 121, 171903 (2022).

[15] Yuichi Oshima, Katsuaki Kawara, Takayoshi Oshima, and Takashi Shinohe, Japan J. Appl. Phys. 59, 115501 (2020).

[16] A. Y. Polyakov, V. I. Nikolaev, A. I. Pechnikov, S. I. Stepanov, E. B. Yakimov, M. P. Scheglov, I. V. Shchemerov, A. A. Vasilev, A. A. Kochkova, A. V. Chernykh, A. V. Chikiryaka and S. J. Pearton, APL Mater. 10, 061102 (2022).

[17] Hiroyuki Nishinaka, Osamu Ueda, Yusuke Ito, Noriaki Ikenaga, Noriyuki Hasuike, and Masahiro Yoshimoto, Japan J. Appl. Phys. 61, 018002 (2022).

[18] Alexander Azarov, Calliope Bazioti, Vishnukanthan Venkatachalapathy, Ponniah Vajeeston, Edouard Monakhov and Andrej Kuznetsov, Phys. Rev. Lett. 128, 015704 (2022)

[19] Alexander Y. Polyakov, Vladimir I. Nikolaev, Sergey A. Tarelkin, Alexei I. Pechnikov, Sergey I. Stepanov, Andrey E. Nikolaev, Ivan V. Shchemerov, Eugene B. Yakimov, Nikolay V. Luparev, Mikhail S. Kuznetsov, Anton A. Vasilev, Anastasiya I. Kochkova, Marina I. Voronova, Mikhail P. Scheglov, Jihyun Kim, and S. J. Pearton, J. Appl. Phys. 129, 185701 (2021).

[20] V. I. Nikolaev, S. I. Stepanov, A. I. Pechnikov, S.V. Shapenkov, M. P. Scheglov, A.V. Chikiryaka, and O. F. Vyvenko, ECS J. Solid State Sci. Technol, 9, 045014 (2020).

[21] A. Y. Polyakov, In-Hwan Lee, A. Miakonkikh, A. V. Chernykh, N. B. Smirnov, I. V. Shchemerov, A. I. Kochkova, A. A. Vasilev, and S. J. Pearton, J. Appl. Phys. 127, 175702 (2020).

[22] for a discussion of the type of gallium oxide wafers available, see the following link, www.tamura-ss.co.jp/en/products

[23] Capacitance spectroscopy of semiconductors, ed. Jian V. Li and Giorgio Ferrari (Pan Stanford Publishing Pte Ltd, Singapore, 2018) 437 pp

[24] M. Tapiero, N. Benjelloun, J.P. Zielinger, S. El Hamd, and C. Noguet, J. Appl. Phys. 54, 4006 (1988)

[25] D.K. Schroder, Semiconductor material and device characterization (Wiley-Interscience, 3rd Edition, New York, 2006)

[26] A. Y. Polyakov, N. B. Smirnov, I. V. Shchemerov, S. J. Pearton, Fan Ren, A. V. Chernykh, and A. I. Kochkova, Appl. Phys. Lett. 113, 142102 (2018)

[27] A. Y. Polyakov, N. B. Smirnov, I. V. Shchemerov, S. J. Pearton, F. Ren, A. V. Chernykh, P. B. Lagov, and T. V.Kulevoy, APL Materials 6, 096102 (2018)

[28] Alexander Y. Polyakov, Nikolai B. Smirnov, In-Hwan Lee, and Stephen J. Pearton, J. Vac. Sci. Technol. B 33, 061203 (2015)

[29] A. Y. Polyakov, N. M. Shmidt, N. B. Smirnov, I. V. Shchemerov, E. I. Shabunina, N. A. Tal'nishnih, In-Hwan Lee, L. A. Alexanyan, S. A. Tarelkin and S. J. Pearton, J. Appl. Phys. 125, 215701(2019).

[30] J. F. Ziegler, M. D. Ziegler, and J. P. Biersack, Nucl. Instrum. Methods Phys. Res. B 268**,** 1818 **(**2010).

[31] A. Dissanayake, M. Elahi, H. X.Jiang, and J. Y. Lin, Phys. Rev. B 45, 24, 13996 (1992)

[32] Amanda Langørgen, Christian Zimmermann, Ymir Kalmann Frodason, Espen Førdestrøm Verhoeven, Philip Michael Weiser, Robert Michael Karsthof, Joel Basile Varley, and Lasse Vines, J. Appl. Phys. 131, 115702 (2022).

[33] Vilde M. Reinertsen, Philip M. Weiser, Ymir K. Frodason, Marianne E. Bathen, Lasse Vines, and Klaus Magnus Johansen, Appl. Phys. Lett. 117, 232106 (2020)

[34] Ribhu Sharma, Mark E. Law, Fan Ren, Alexander Y. Polyakov and S. J. Pearton, Vac. Sci. Technol. A 39, 060801(2021).

Table I. Implant parameters used in the present study.

Implants		Energy (keV)	Dose (ions/cm^2)	T_i (^{o}C)
initial	$^{69}Ga^+$	1700	6×10^{15}	RT
additional	$^{28}Si^+$	300	1×10^{15}	RT
		36	2×10^{14}	200
				400

FIGURE CAPTIONS

Fig. 1 (a) RBS/C spectra and (b) corresponding XRD Θ-2Θ scans of the Ga_2O_3 samples co-implanted with Ga+Si ions at different temperatures as indicated in the legend. The virgin (unimplanted) RBS/C is shown for comparison.

Fig. 2 RBS/C spectra of the Ga_2O_3 samples co-implanted with Ga+Si ions at 200 °C before and after different anneals as indicated in the legend. The virgin (unimplanted) spectra are shown for comparison.

Fig. 3 (Color online) (a) I-V characteristics for the sample implanted with Ga and Si (Si implantation at 400^{o}C) at room temperature in the dark (black line), at room temperature with 4.5 eV photons illumination (violet line), at 420K in the dark (red line); (b) the spectral dependence of photocurrent at 50V (open squares) and the current measured after the light switched off; (c) the temperature dependence of current at 50V measured upon heating up from room temperature after 10 minutes illumination with 4.5 eV photons (red line) and the temperature dependence measured upon cooling down from 420K.

Fig. 4 (Color online) (a) PICTS signal measured at 50V with 4.5 eV photon energy LED excitation (5 s long pulse) for t1/t2=0.2 s/1 s (black line), t1/t2=0.5 s/2.5s (red line), 1.2 s/6s (blue line), t1/t2=2.2 s/12 s (olive line); (b) the same with t1/t2=2s/10 s (black line),3.2s/16s (red line), 4.8s/24 s (blue line), 6.8 s/34 s (olive line).

Fig. 5 (color online) (a) I-V characteristics measured for the sample implanted with Ga, with Si at 400^{o}C, and treated in hydrogen plasma; measurements at 298 K, 400K, 156K; (b) C-f characteristics measured at different temperatures; $1/C^2$ - voltage measured at room temperature at 10 kHz

Fig. 6 (Color online) The temperature dependence of current measured at 2V upon heating up from room temperature after illumination with 4.5 eV photons (red line) and during cooling down from high temperature in the dark.

Fig. 7 (Color online) (a) The spectral dependence of reverse current at -5V (solid squares) and the current measured after switching the light off and applying 5V direct voltage for 10 s (open circle); (b) the spectral dependence of photocapacitance on the C-f plateau normalized by the dark capacitance (solid squares) and normalized photocapacitance measured after switching the light off and applying forward voltage of 5V for 5 s (open circle).

Fig. 8 (Color online) (a) The temperature dependence of dC/dT for several probing frequencies; (b) CDLTS spectra measured with reverse bias -2V and forward bias pulse of 1V (1 s long) (solid line is for t1/t2 windows of 0.15 s/1.5 s, dashed line is for 2.55 s/ 25.5 s; (c) DLTS spectra measured at 10 kHz with reverse bias of -1V and forward bias pulse 1V (1 s long) shown for time windows 0.5s/5s (solid line) and 2.5 s/25 s (dashed line).

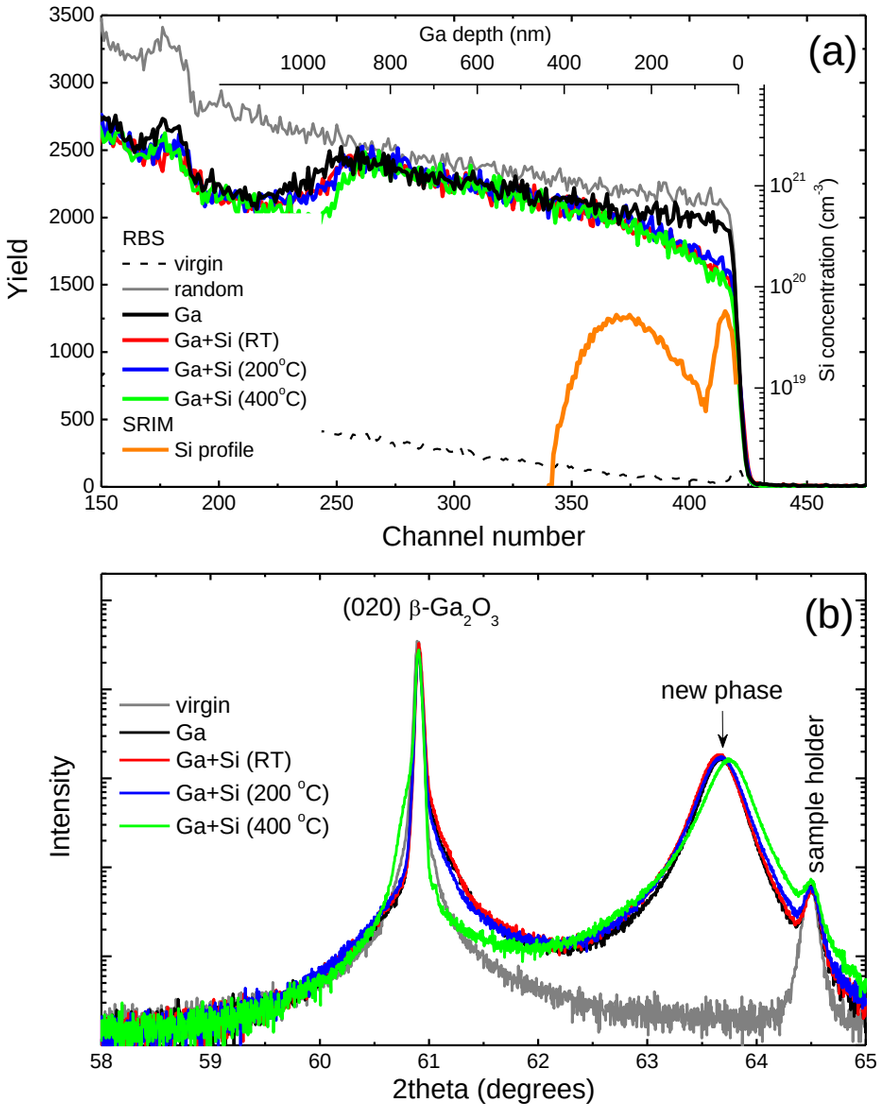

Fig. 1 (a) RBS/C spectra and (b) corresponding XRD Θ-2Θ scans of the Ga_2O_3 samples co-implanted with Ga+Si ions at different temperatures as indicated in the legend. The virgin (unimplanted) RBS/C

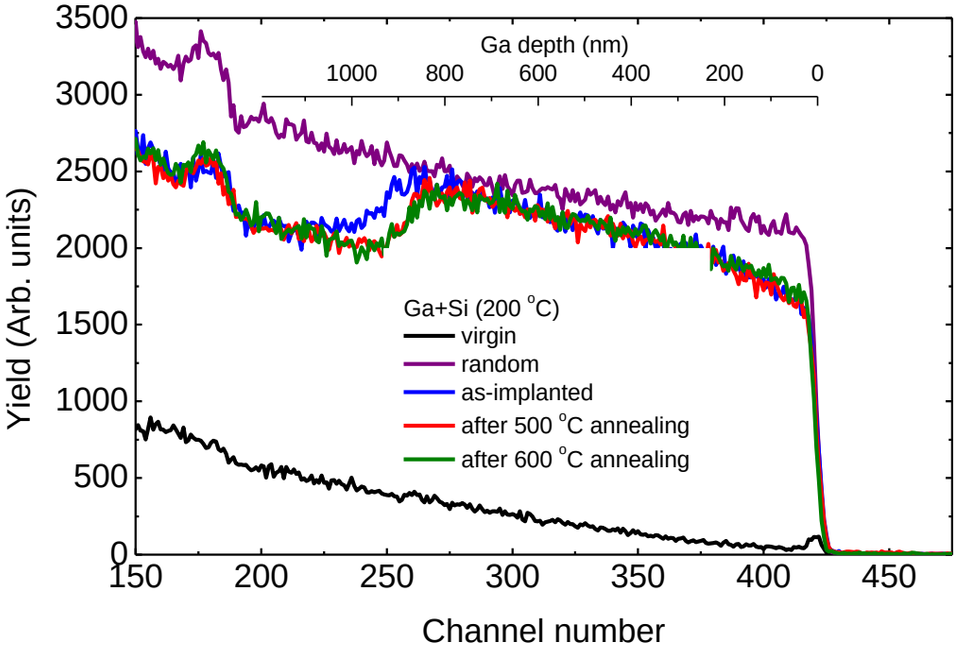

Fig. 2 RBS/C spectra of the Ga_2O_3 samples co-implanted with Ga+Si ions at 200 °C before and after different anneals as indicated in the legend. The virgin (unimplanted) spectra are shown for comparison.

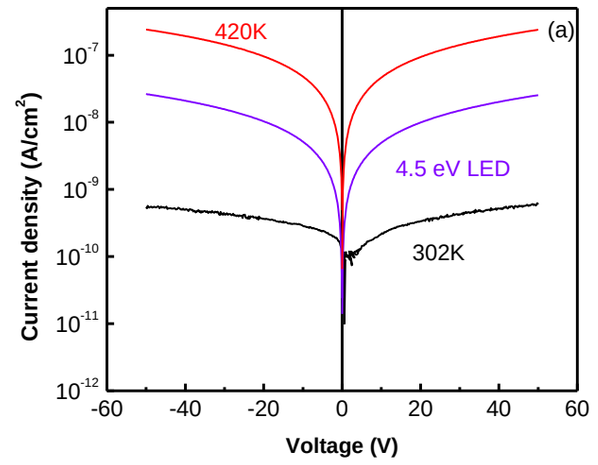

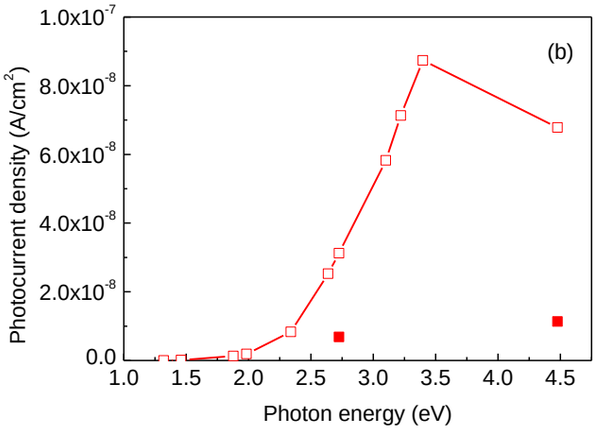

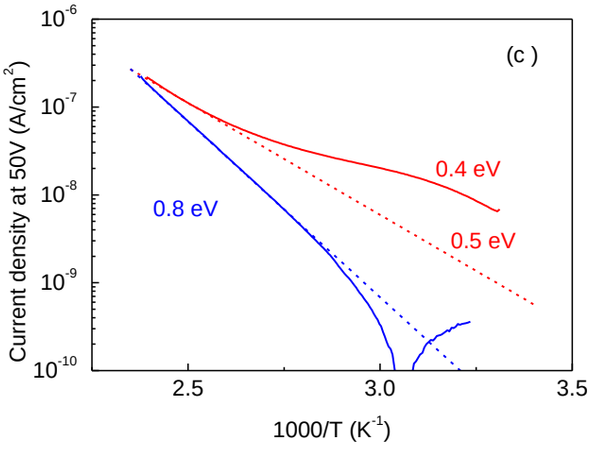

Fig. 3 (Color online) (a) I-V characteristics for the sample implanted with Ga and Si (Si implantation at 400^{o}C) at room temperature in the dark (black line), at room temperature with 4.5 eV photons illumination (violet line), at 420K in the dark (red line); (b) the spectral dependence of photocurrent at 50V (open squares) and the current measured after the light switched off; (c) the temperature

Journal of Applied Physics

AIP Publishing

dependence of current at 50V measured upon heating up from room temperature after 10 minutes illumination with 4.5 eV photons (red line) and the temperature dependence measured upon cooling down from 420K

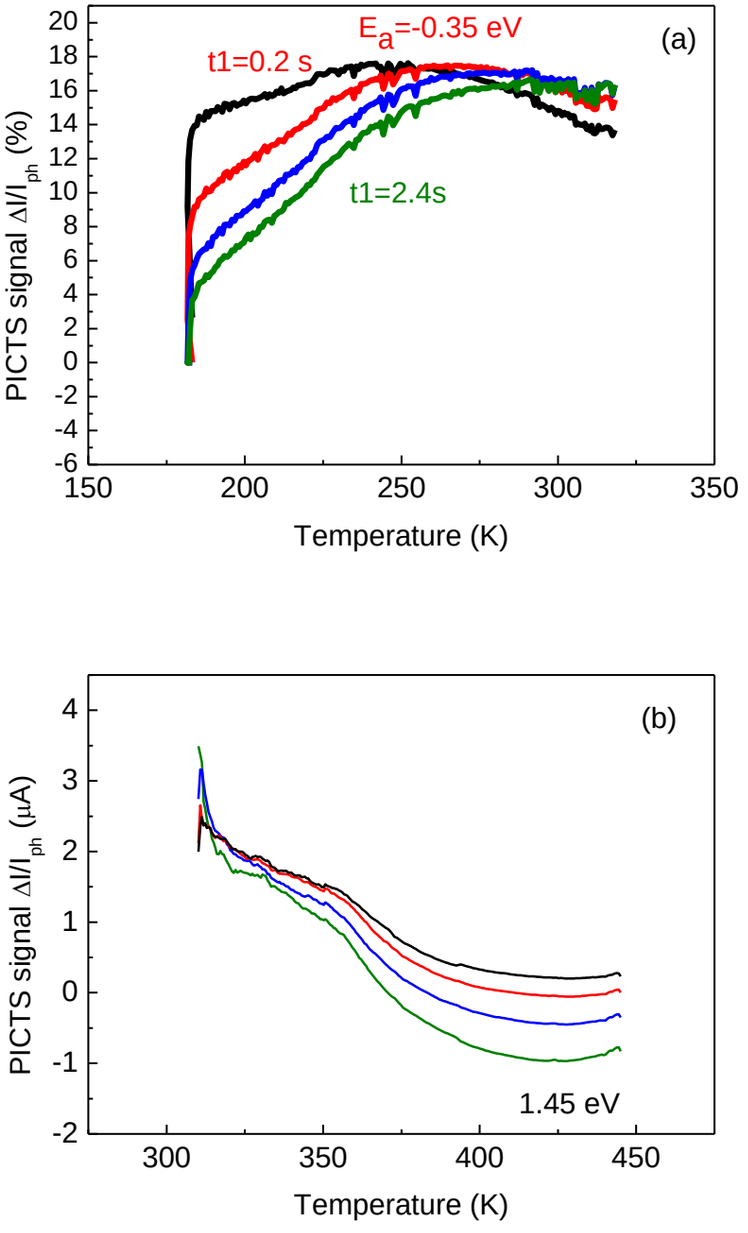

Fig. 4 (Color online) (a) PICTS signal measured at 50V with 4.5 eV photon energy LED excitation (5 s long pulse) for t1/t2=0.2 s/1 s (black line), t1/t2=0.5 s/2.5s (red line), 1.2 s/6s (blue line), t1/t2=2.2 s/12 s (olive line); (b) the same with t1/t2=2s/10 s (black line),3.2s/16s (red line), 4.8s/24 s (blue line), 6.8 s/34 s (olive line).

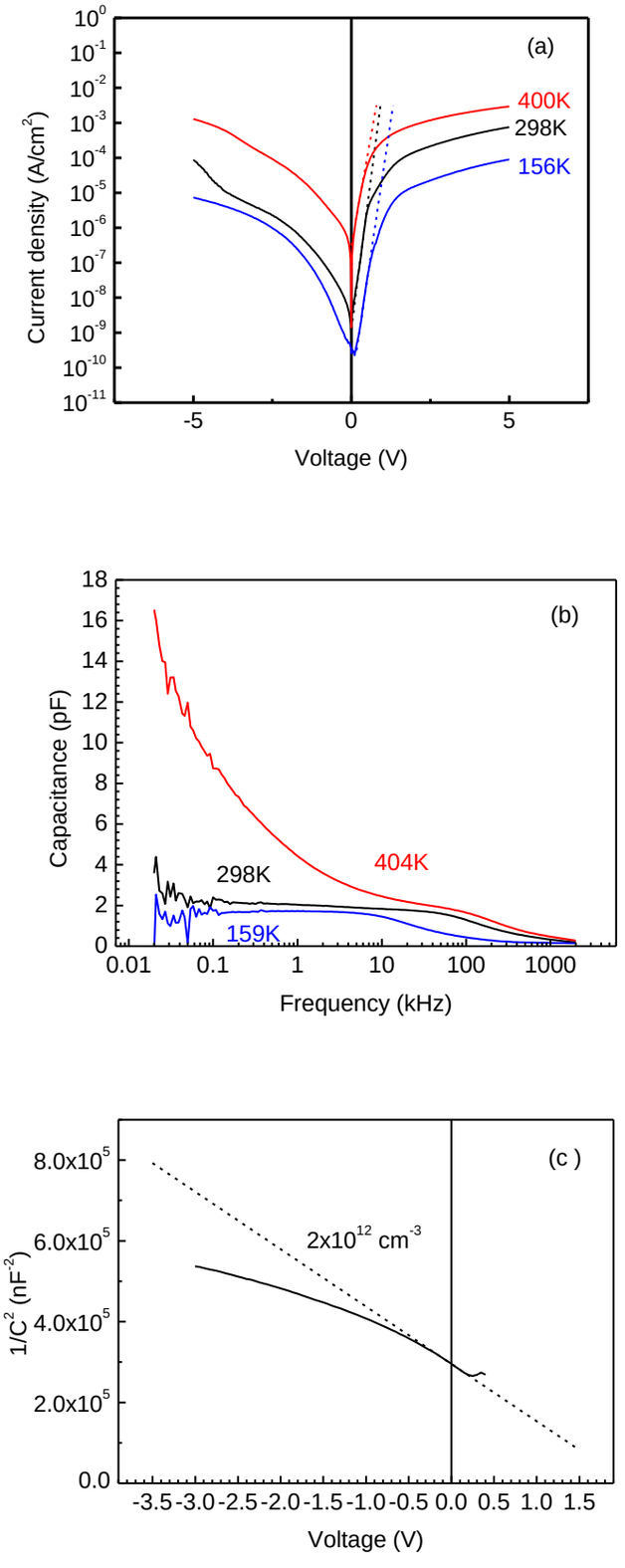

Fig. 5 (color online) (a) I-V characteristics measured for the sample implanted with Ga, with Si at 400^{o}C, and treated in hydrogen plasma, measurements at 298 K, 400K, 156K; (b) C-f

characteristics measured at different temperatures; 1/C2 versus voltage measured at room temperature at 10 kHz.

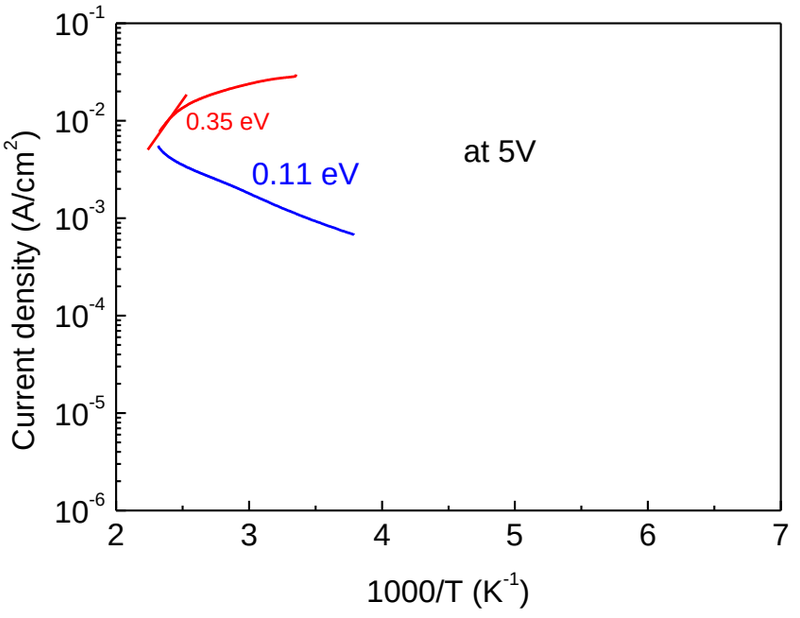

Fig. 6 (Color online) The temperature dependence of current measured at 2V upon heating up from room temperature after illumination with 4.5 eV photons (red line) and during cooling down from high temperature in the dark.

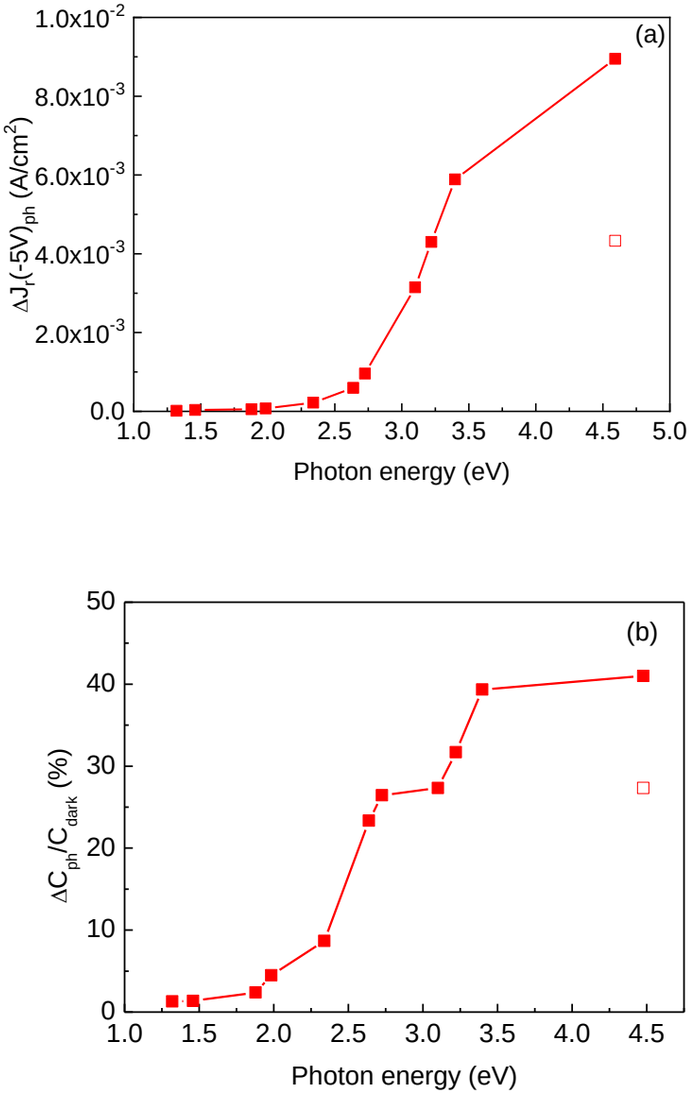

Fig. 7 (Color online) (a) The spectral dependence of reverse current at -5V (solid squares) and the current measured after switching the light off and applying 5V direct voltage for 10 s (open circle); (b) the spectral dependence of photocapacitance on the C-f plateau normalized by the dark capacitance (solid squares) and normalized photocapacitance measured after switching the light off and applying forward voltage of 5V for 5 s (open circle).

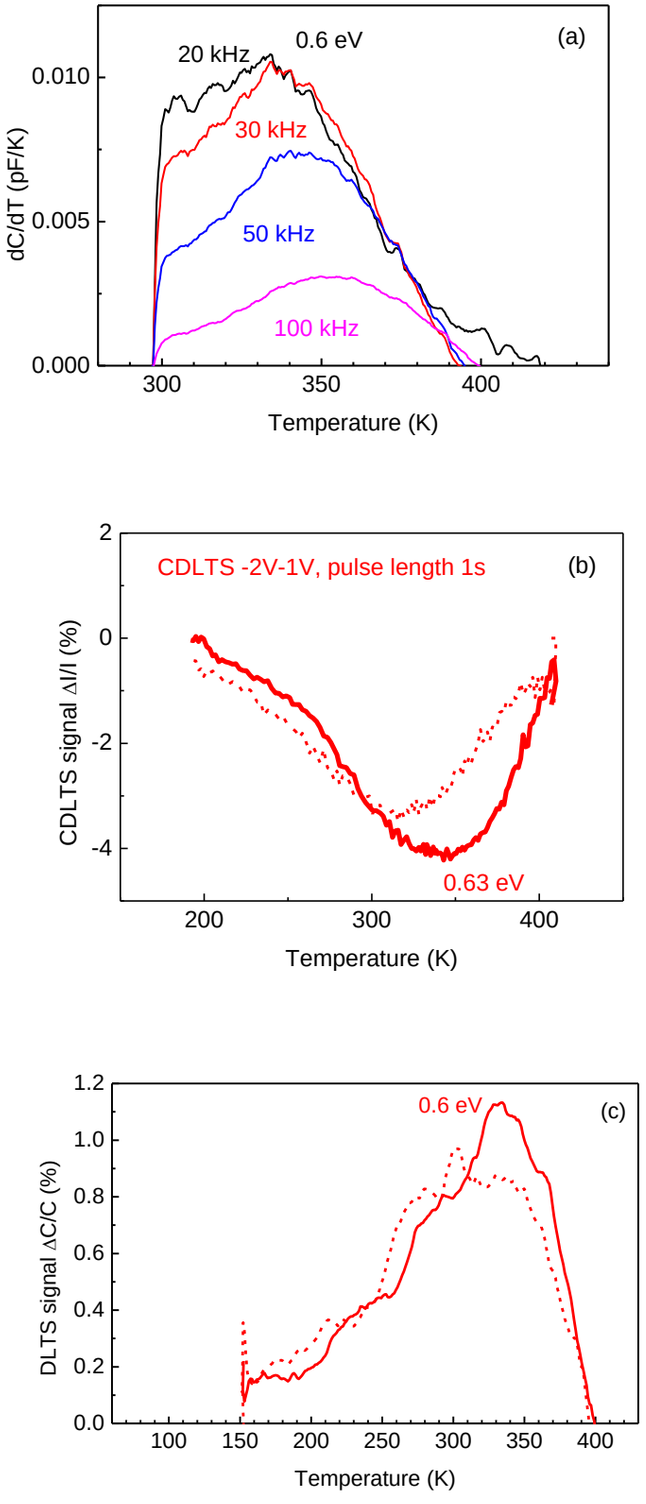

Fig. 8 (Color online) (a) The temperature dependence of dC/dT for several probing frequencies; (b) CDLTS spectra measured with reverse bias -2V and forward bias pulse of 1V (1 s long) (solid line is for t1/t2 windows of 0.15 s/1.5 s, dashed line is for 2.55 s/ 25.5 s; (c)

DLTS spectra measured at 10 kHz with reverse bias of -1V and forward bias pulse 1V (1 s long) shown for time windows 0.5s/5s (solid line) and 2.5 s/25 s (dashed line).

AIP Publishing

Journal of Applied Physics

ACCEPTED MANUSCRIPT

This is the author's peer reviewed, accepted manuscript. However, the online version of record will be different from this version once it has been copyedited and typeset.
PLEASE CITE THIS ARTICLE AS DOI: 10.1063/5.0133181

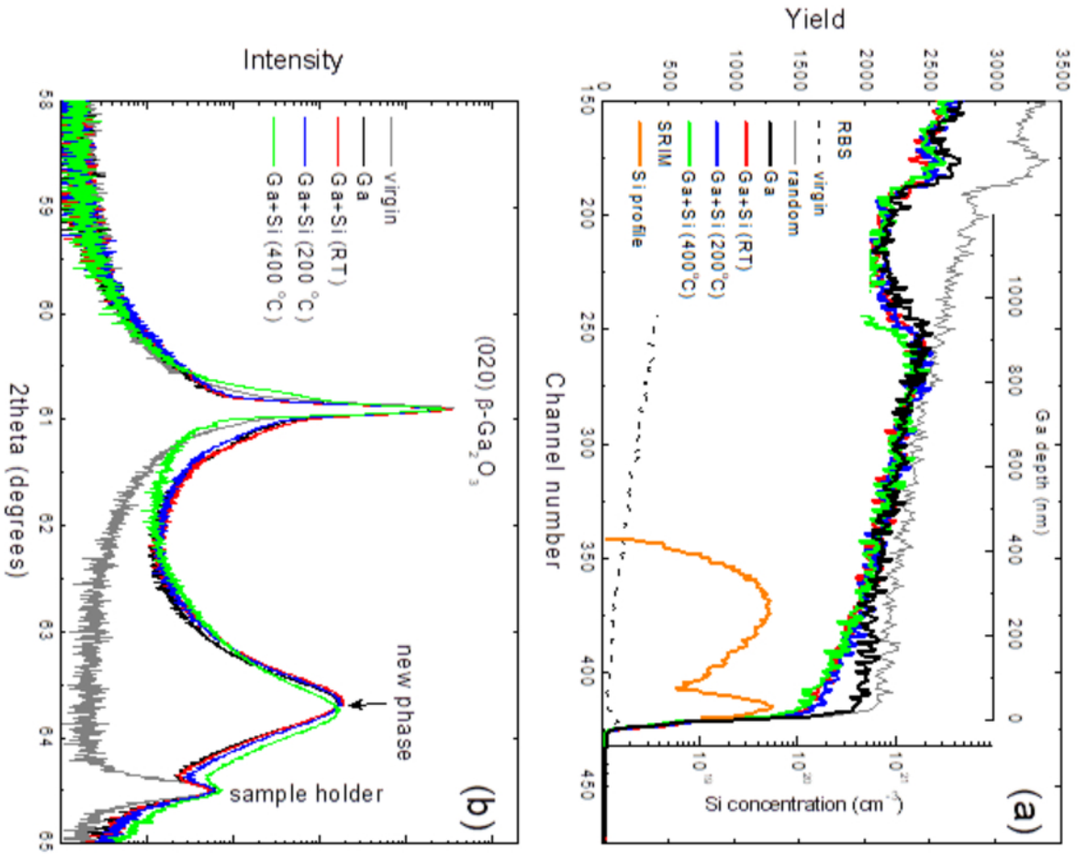

AIP Publishing

Journal of Applied Physics

ACCEPTED MANUSCRIPT

This is the author's peer reviewed, accepted manuscript. However, the online version of record will be different from this version once it has been copyedited and typeset.
PLEASE CITE THIS ARTICLE AS DOI: 10.1063/5.0133181

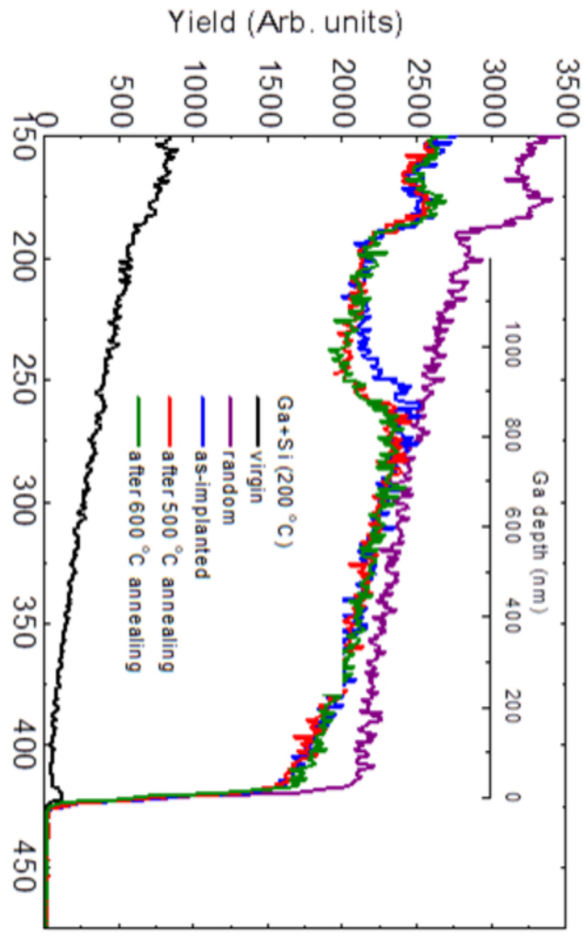

AIP Publishing

Journal of Applied Physics

ACCEPTED MANUSCRIPT

This is the author's peer reviewed, accepted manuscript. However, the online version of record will be different from this version once it has been copyedited and typeset.
PLEASE CITE THIS ARTICLE AS DOI: 10.1063/5.0133181

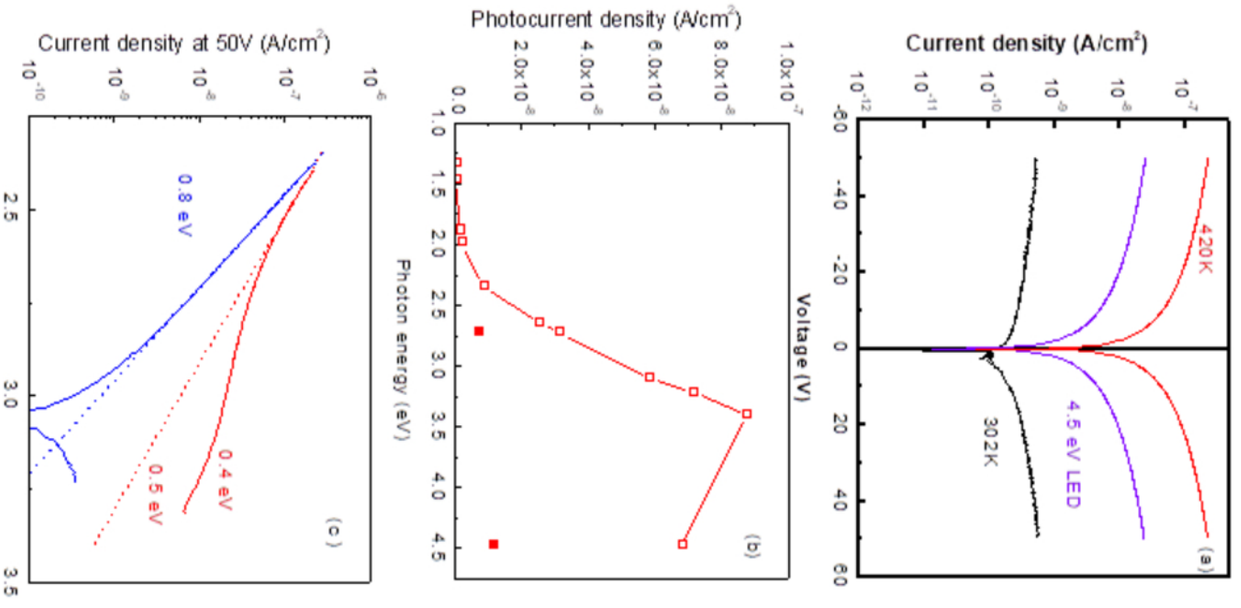

AIP Publishing

Journal of Applied Physics

ACCEPTED MANUSCRIPT

This is the author's peer reviewed, accepted manuscript. However, the online version of record will be different from this version once it has been copyedited and typeset.
PLEASE CITE THIS ARTICLE AS DOI: 10.1063/5.0133181

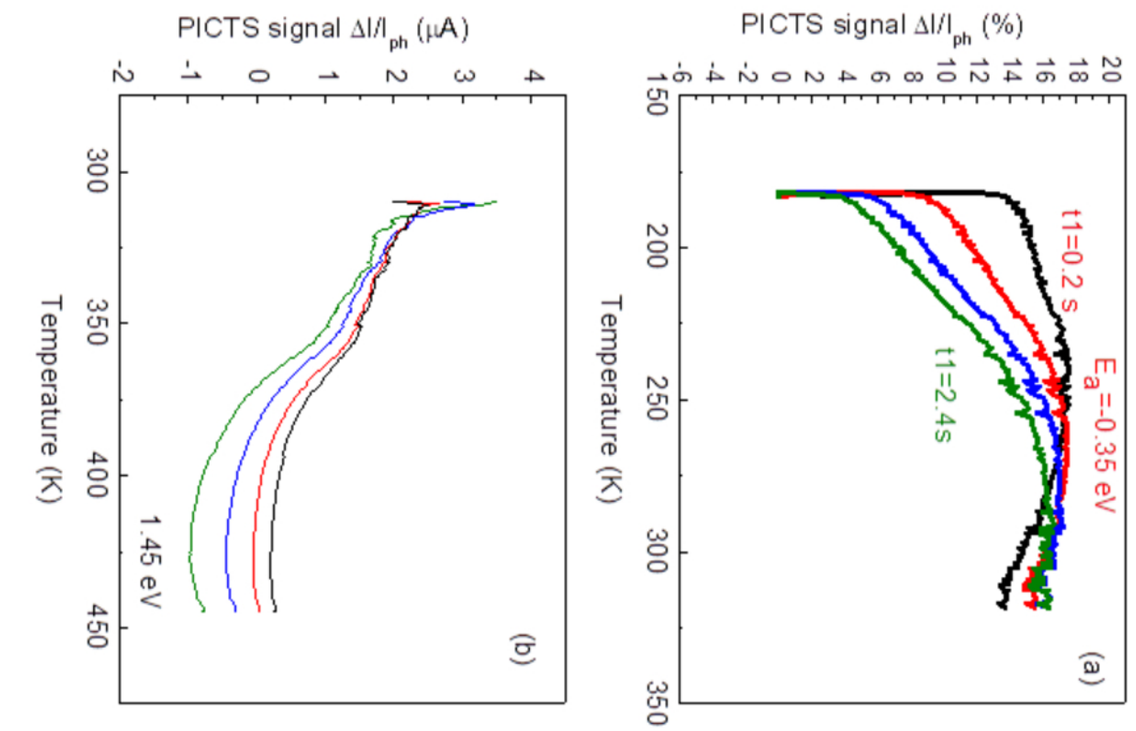

AIP Publishing

Journal of Applied Physics

ACCEPTED MANUSCRIPT

This is the author's peer reviewed, accepted manuscript. However, the online version of record will be different from this version once it has been copyedited and typeset.
PLEASE CITE THIS ARTICLE AS DOI: 10.1063/5.0133181

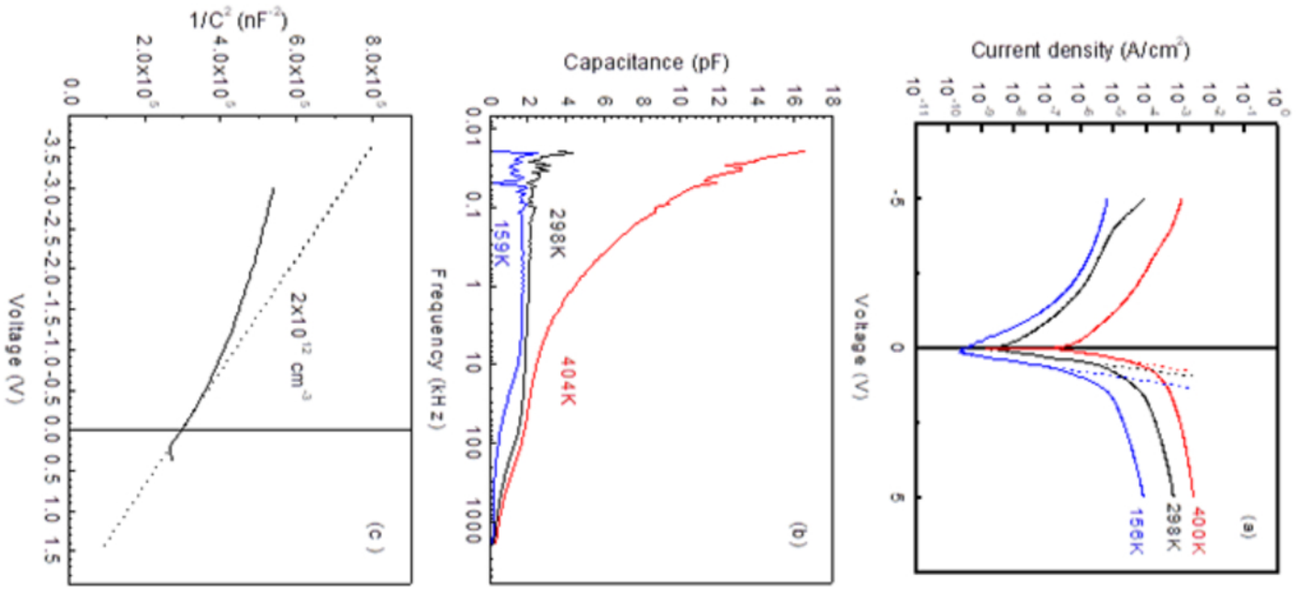

AIP Publishing

Journal of Applied Physics

ACCEPTED MANUSCRIPT

This is the author's peer reviewed, accepted manuscript. However, the online version of record will be different from this version once it has been copyedited and typeset.
PLEASE CITE THIS ARTICLE AS DOI: 10.1063/5.0133181

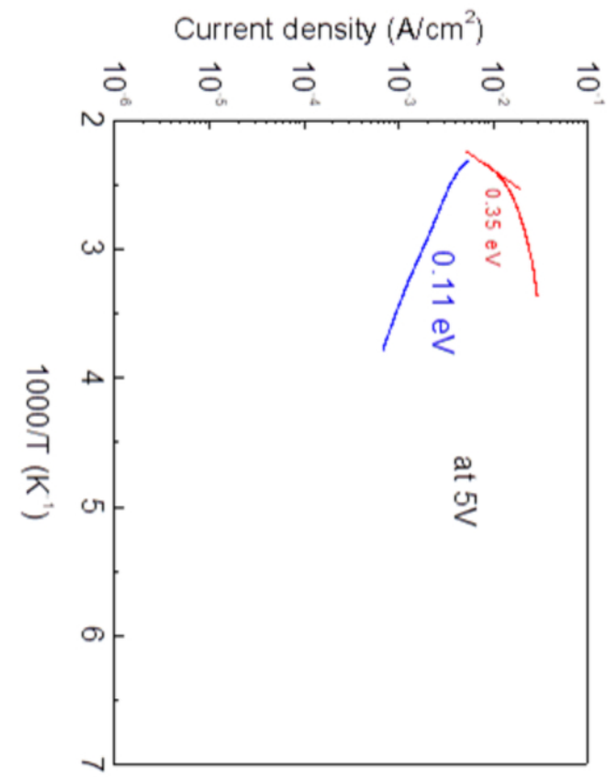

AIP Publishing

Journal of Applied Physics

ACCEPTED MANUSCRIPT

This is the author's peer reviewed, accepted manuscript. However, the online version of record will be different from this version once it has been copyedited and typeset.
PLEASE CITE THIS ARTICLE AS DOI: 10.1063/5.0133181

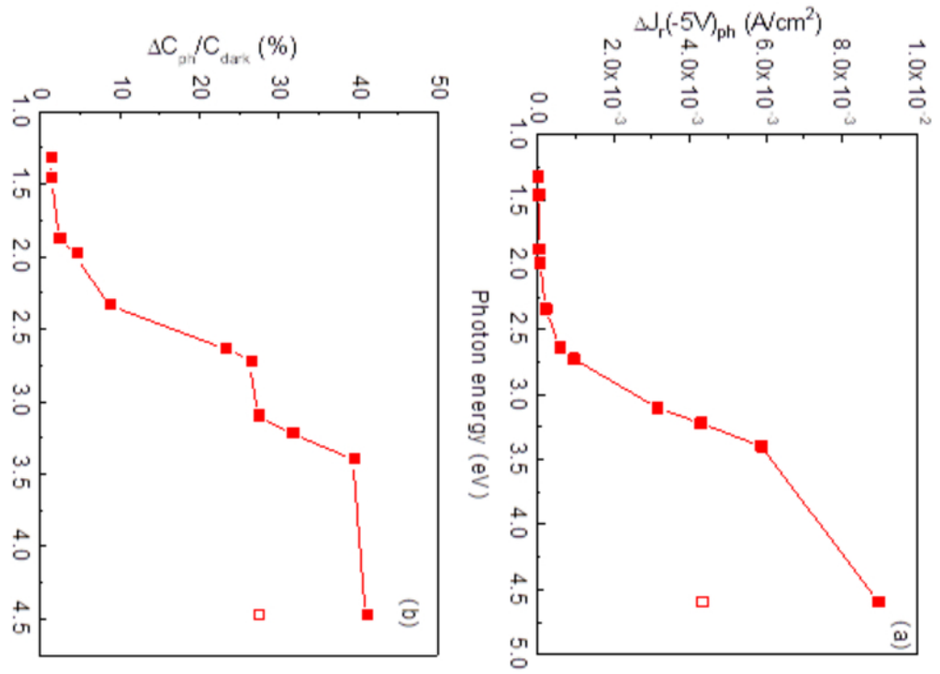

AIP Publishing

Journal of Applied Physics

ACCEPTED MANUSCRIPT

This is the author's peer reviewed, accepted manuscript. However, the online version of record will be different from this version once it has been copyedited and typeset.
PLEASE CITE THIS ARTICLE AS DOI: 10.1063/5.0133181